Tech Science Press

Hybrid Deep Learning-Improved BAT Optimization Algorithm for Soil Classification Using Hyperspectral Features

S. Prasanna Bharathi[1,2], S. Srinivasan[1,*], G. Chamundeeswari[1] and B. Ramesh[1]

[1]Saveetha School of Engineering, Saveetha Institute of Medical and Technical Sciences, Saveetha Nagar, Thandalam, Chennai, 602105, Tamilnadu, India
[2]Department of Electronics and Communication Engineering, College of Engineering & Technology, SRM Institute of Science and Technology, Vadapalani Campus, Chennai, 600026, India
*Corresponding Author: S. Srinivasan. Email: srinivasan.me.03@gmail.com
Received: 21 January 2022; Accepted: 02 March 2022

Abstract: Now a days, Remote Sensing (RS) techniques are used for earth observation and for detection of soil types with high accuracy and better reliability. This technique provides perspective view of spatial resolution and aids in instantaneous measurement of soil's minerals and its characteristics. There are a few challenges that is present in soil classification using image enhancement such as, locating and plotting soil boundaries, slopes, hazardous areas, drainage condition, land use, vegetation etc. There are some traditional approaches which involves few drawbacks such as, manual involvement which results in inaccuracy due to human interference, time consuming, inconsistent prediction etc. To overcome these draw backs and to improve the predictive analysis of soil characteristics, we propose a Hybrid Deep Learning improved BAT optimization algorithm (HDIB) for soil classification using remote sensing hyperspectral features. In HDIB, we propose a spontaneous BAT optimization algorithm for feature extraction of both spectral-spatial features by choosing pure pixels from the Hyper Spectral (HS) image. Spectral-spatial vector as training illustrations is attained by merging spatial and spectral vector by means of priority stacking methodology. Then, a recurring Deep Learning (DL) Neural Network (NN) is used for classifying the HS images, considering the datasets of Pavia University, Salinas and Tamil Nadu Hill Scene, which in turn improves the reliability of classification. Finally, the performance of the proposed HDIB based soil classifier is compared and analyzed with existing methodologies like Single Layer Perceptron (SLP), Convolutional Neural Networks (CNN) and Deep Metric Learning (DML) and it shows an improved classification accuracy of 99.87%, 98.34% and 99.9% for Tamil Nadu Hills dataset, Pavia University and Salinas scene datasets respectively.

Keywords: HDIB; bat optimization algorithm; recurrent deep learning neural network; convolutional neural network; single layer perceptron; hyperspectral images; deep metric learning

1 Introduction

Over the past few years, Brazil has become a pioneer in horticulture because of its venture into new agrarian crops, upgradation & automation of machinery and excellent endeavors to address the problems faced by the agriculturists [1,2]. To proceed with this development, Brazil must practice new methodologies for utilizing and overseeing uncultivated land zones. Most changes occurring in the soil are moderate and subtle especially when seen in the time span of human life. Be that as it may, due to natural calamities, it results in disintegration which brings quantifiable changes to the land mass [3]. The progressions are principally in the structure and organization of the material and such changes are referred to as 'basic changes'. Soil is the base for each generation framework and information on their properties, degree and spatial dispersion is critical before we start cultivating any products in that land mass [4–7]. More than 90% of world's nourishment issues are related to soil. Soil asset stock gives an understanding into the possibilities and constraint of soil for its viable use. In soil mapping we can experience stock of various soils, their type and nature and it additionally gives data regarding land structure, vegetation. Suitable evidence on the type of soils is essential in creating a plan for land use in farming, water system, waste management and so on. Standard soil study collates data about soil in an efficient way with respect to their degree, constraints and to group them. Satellite remote sensing and GIS methods are the procedures which are used as of late in deciding the quantitative portrayal of the landscape highlights and geomorphologic mapping [8,9]. Over the years remote sensing [10] has grown as a fundamental tool in soil asset study which helps to increase the ideal land utilization plan for economic development at scale running from provincial to smaller scale levels [11]. The variables associated with physiographic forms pretty much compare to the elements of soil development. Hyperspectral information provides procedures such as collinear indicator factors, which is, autonomous from the independent variable, and these images also has a disadvantage. To solve this problem, dimensionality reduction technique is the standard procedure [12,13]. Partial Least Squares Regression (PLSR) [14,15], for instance, extends the information into a low-dimensional space shaped by a lot of symmetrical factors with an intention to increase the covariance among indicators and target variable(s). PLSR is the most widely recognized multivariate data analysis, albeit different methodologies have additionally been applied effectively. Customary techniques for distinguishing and checking of salt influenced soils can outline saltiness just up to a limited degree. These techniques are costly, tedious and require large number of tests from a region to describe spatial changeability, which limits the practice of these techniques for contemplating huge and non-uniform territories [16,17]. Different RS images are by and large generally utilized in portrayal and mapping of salt influenced soils including ethereal photos, Multi Spectral (MS) and HS remote sensing images. Soil saltiness mapping is a troublesome assignment to perform, due to the high impact of different soil physical and synthetic properties (for example dampness, surface harshness, natural issue) on soil reflectance. Prior to the RS techniques, observing and mapping of salt influenced soils over large regions were broadly and effectively attempted utilizing broadband multispectral information [18].

Contributions of this paper are that, we propose a Hybrid Deep Learning-Improved BAT optimization algorithm (HDIB) for soil classification using RS hyperspectral features. Initially, we introduce an improved BAT optimization algorithm for feature extraction of both spectral-spatial features and removed by choosing physically pure pixels from hyperspectral image, after which we are using a priority stacking approach for combining the spectral vector with spatial vector as training samples. Thirdly, we have introduced a recurrent deep learning neural network which is used to acquire the discerning metric aimed at the cataloguing of hyperspectral images, which improves the reliability of classification. Finally, the HDIB algorithm is compared with the other existing techniques in terms of classification accuracy.

The paper is arranged in the following sequence: In part I, we explain overview of soil classification using RS. In part II, we discuss the issues of soil classification and RS based on some illustrative

examples. The analysis of the various issues prevalent in the previous methods and the system model design are briefed in Section III and it briefs about the proposed algorithm. In part IV we have discussed about the performance analysis and the description of the dataset and in part V of the paper is used to discuss about the implementation aspects and the results. Finally, Section VI outlines the major conclusions of this research.

2 Related Works

Enormous research has been presented in the paper for the soil classification using RS hyperspectral features. Some of the latest work has been reviewed below.

Neto et al. [19] have proposed Artificial Neural Network (ANN) for analysis of soil which have been degraded over the times and its recuperation due to gypsum & lime deposits. The examined soil was named Oxisol & the parameters which was taken into consideration were: soil porosity, soil thickness and soil resistance. The Backpropagation method is the type of ANN which is applied in this investigation, which is made out of 2 layers, the center & the output layer, considering the supervised training. The system designed has 4 inputs, which are the characteristics of the soil. In the center layer, the system consists of 10 neurons and the final layer which is the output layer consists of a single neuron, having the capability of analyzing if the soil has Recuperated (R), Partially Recuperated (PR) or Not Recuperated (NR). After analysing the performance of the ANN, the network was verified to have acquired satisfactory training demonstrating low Mean Square Error (MSE) which is used to classify the degraded soils.

Wu et al. [20] have used the data of Normalized Difference Vegetation Index (NDVI) which was considered over an uneven terrain using the LANDSAT images which was devoid of clouds. The Landscape indicators like Wetness Index of the Topography, elevation and slope were obtained from a computerized map with resolution of upto 30 m. Models with various criteria like pure NDVI, pure topography & stratum, NDVI + Stratum and Topography was created. By and large Receiver Operating Characteristics (ROC), kappa measurement, and the Area under ROC curve (AUC) was analysed to assess classification accuracy. The results were very encouraging and it had great impact on the outputs. Amongst all the models which were considered, the model with NDVI + Stratum and Topography had the best performance with respect to AUC, Kappa Measurement & accuracy of 0.907, 0.918, and 0.975 respectively. The findings will give important data to evaluate the nature of biological condition utilizing RS images. Gao et al. [21] have proposed environmental quality grade techniques that are used for mapping or assessing global means, which is basically centered on assessing the connections between unsampled areas & the edges that arrange the earth quality grades. These groupings must utilize a testing format enhancement technique to disperse extra inspecting units hooked on zones with an elevated danger of misclassification. To determine these issues, this exertion gives an extra specimen format improvement technique that at first progresses an inaccuracy index by constructing a multi-Gaussian prototypical for the unsampled locations which gives the error and variances of it which is then used to calculate the threshold assessment probability in the Gaussian curve. The regular error records of entire areas in the investigation territory are then customary as the detachment capacity of the extra testing format streamlining, and the spatial reenacted strengthening is received to acquire the upgraded examining design by limiting the objectivity work.

Ghosh et al. [22] have proposed Neuro-Fuzzy (NF) technique which is a classification-based algorithm, that helps in detecting the different soil classes from a large soil database. This classification technique is a Fuzzification method that is based on detecting the different soil classes by looking into the feature-wise characteristics of the image dataset under investigation. The Fuzzification method creates a Membership Matrix whose elements are the inputs to the neural network. This technique has been applied to the Forset Covertype, Wilt for soil and Statlog Landsat Satellite database. This paper is used to find classify

the types of soils using Fuzzification method and comparing the results with Support Vector Machine (SVM), K-Nearest Neighbour, Adaptive NF Inference system and Radial Basis Function Network (RBFN). Using the NF technique, the Accuracy, Recall, Precision, Kappa Statistic, False Positive Rate (FPR), Area Under Curve (AUC), F measure, Root Mean Square Error (RMSE), True Positive Rate (TPR) were calculated and the proposed NF method has effectively proved its supremacy over the above mentioned 4 algorithms. Yang et al. [23] have proposed Minimum Noise Fractions (MNFs) method which is integrated with a Fast and Adaptive Bidimensional Empirical Mode Decomposition (FABEMD) to resolve the scattered pixel issue while working with the HS images which is created by the atmospheric scattering and noise. The paper is based on the Indiana Pine Dataset to increase the characterization precision of airborne infrared spectrometer HS images. The MNF + FABEMD breaks down a HS image into a few Bidimensional Intrinsic Mode Functions (BIMF) & remnant picture. The initial four BIMFs are eliminated & the rest of BIMF's are used to integrate to create an informative image which is then classified using SVM.

Xue et al. [24] The image classification on HS images has its own challenges because of the usage of different types of HS data. As of late, spectral-spatial methodologies were created by together dealing with the spectra and spatial data. This paper shows a totally unique methodology from a subpixel target location's viewpoint. It executes in 4 phases - preprocessing phase, a recognition stage, that generates subpixel target maps, followed by an iterative phase, that builds up an Iterative Constrained Energy Minimization (ICEM) by applying the Gaussian filters to detect the spatial data. Finally, the Gaussian filtered images are fed into the BSNE band pictures to reclaim CEM in an iterative way. Pike et al. [25] have proposed a classification method that is used for detecting the cancerous cells from the healthy ones by combining the spectral and spatial data in the HS images. This paper is based on the Minimum Spanning Forest (MSF) which in turn uses a band selection method for distinguishing the cancerous cells and the healthy cells. A SVM Classifier has been trained to create a pixel wise probability map for the cancerous and healthy tissues which is used later to calculate for the various band range in the HS data & finally selecting the optimal band after calculation. The MSF method is finally used to segment the HS images based on the spatial and spectral information. Guo et al. [26] proposed a multichannel optical imaging sensor that has expanded usage of HS data for RS. For HS data, a training dataset is important for guaranteeing exceptional accuracy. Nonetheless, in RS, labelled sample data are difficult to obtain and its often costly. This makes Active Learning (AL) a significant method in image analysis. AL symbolizes to effectively construct an efficient library dataset that provides more information for classifying the images. A spatial-spectral AL technique is created that coordinates spectral and spatial highlights extricated from super pixels in an AL system.

Li et al. [27] The extraordinary feature extraction potential that the Deep CNN (DeCNN) possesses makes it as one of the promising methods for High Spatial Resolution Remote Sensing (HSRRS) scene classification. High resolution datasets are needed to achieve best classification performance and to avoid overfitting, during the training of the DeCNN model, but its performance is limited due to the lack of high-quality data sets. To solve this problem, a method to classify a HSRRS image scene using Transfer Learning (TL) and the DeCNN (TL-DeCNN) model in multiple HSRRS scene samples is proposed. In particular, 3 typical DeCNN's of Inception V3, ResNet and VGG19 which are all trained on the ImageNet2015, the convolutional layer's weight for TL-DeCNN is transferred. So, TL-DeCNN has to configure its classification module on several samples captured from the HSRRS scene in different periods. Experiment results show that the proposed TL-DeCNN technique provides dominance results without fitting problem compared to ResNet50, VGG19 and InceptionV3.

Tan et al. [28] Semantic Road and street segmentation in RS images utilizes DL. With the use of the CNN algorithms, the features that are present within the Convolution Layer (CL) that have more semantic information ends up being more noteworthy for segmentation of roads. The problem that is addressed in this paper is that the spatial resolution of CL gets reduced as the CNN deepens which results

in loss of important information of the roads. Many research has gone into the semantic segmentation to classify roads. The paper proposes a novel end-to-end segmentation methodology which recognizes the various levels in the CL which would precisely detect the road edges, turns and shapes and this model comprises of a decoder and an encoder. The encoder encodes the picture and it is a classification network which would use VGGNet and ResNet. The decoder comprises of scale fusion and sensitive modules. The scale fusion module integrates the semantic information of higher and lower level. In a scale sensitive module, a weight tensor is set which ensures that the features having more information are more prominent. This methodology improves the accuracy & it is implemented on Massachusetts Roads dataset.

3 Problem Methodology and System Model

This part explains about the identification of the problem of existing soil classification using RS hyperspectral features, followed by the proposed system model.

3.1 Problem Methodology

Cao et al. [29] have proposed a Deep Metric Learning (DML) neural system which is basically used for assigning small distances for the samples which are present in the same class and large distances for the samples present in the different classes. The non-linear relationships between the samples cannot be captured by the various old metric learning techniques. This paper uses the Deep Neural Network (DNN) which is used to learn about metrics which are discriminating for classifying HS images. The heaviness regularization is likewise acquainted through break from the over-fitting. To improve the classification of the system further, the spectral and spatial data are both consolidated together. The most famous learning techniques for example DML neural system can viably get familiar with the picture which is mutually unaided and administered route in state of marked information is rare. In view of the attribute of HS images, DML could give another plan to separating a more grounded enlightening capacity of HS image classification with constrained information [30–33]. Owing to its elevated discriminative capability to categorize besides extricate diverse materials; HS imaging has stood in RS to scrutinize the earth surface for various applications such as military, mining, atmosphere monitoring, agriculture, etc. Moreover, HS imaging can also be used in applications like biomedicine, food security, biometrics, quality control [34]. Soil cataloguing is problematic to envisage the soil reflectance by means of physical prototypes besides theories due to the probability of quantitative translation of the reflectance spectrum of the multi-mineral is quite cumbersome. In addition, the theoretical consequences do not habitually approve with reality besides are not lawful for the impost of soil possessions. Hence, we necessitate instituting a new technique that is capable to disclose the multifaceted relationships amongst reflectance from various minerals present in the soil and exclusively in very large areas [35–39].

3.2 System Model - Hybrid Deep Learning-Improved Bat Optimization Algorithm For Soil Classification Using Hyperspectral Features (HDIB)

To overcome this draw backs, we propose a hybrid deep learning-improved BAT optimization algorithm (HDIB) for soil classification using remote sensing hyperspectral features.

1. In HDIB, first we propose an improved BAT optimization algorithm for feature extraction of both spectral-spatial features and removed by picking physically pure pixels from HS image.
2. Second, Spectral-spatial vector as training illustrations is attained by way of merging spatial vector with spectral vector by means of precedence assembling methodology. Then, a recurrent deep learning neural network is applied to acquire the discerning metric aimed at classifying the HS images.

3. Finally, the performance of proposed HDIB (shown in Fig. 1) based soil classifier is compared with the existing state-of-art techniques with respect to classification precision.
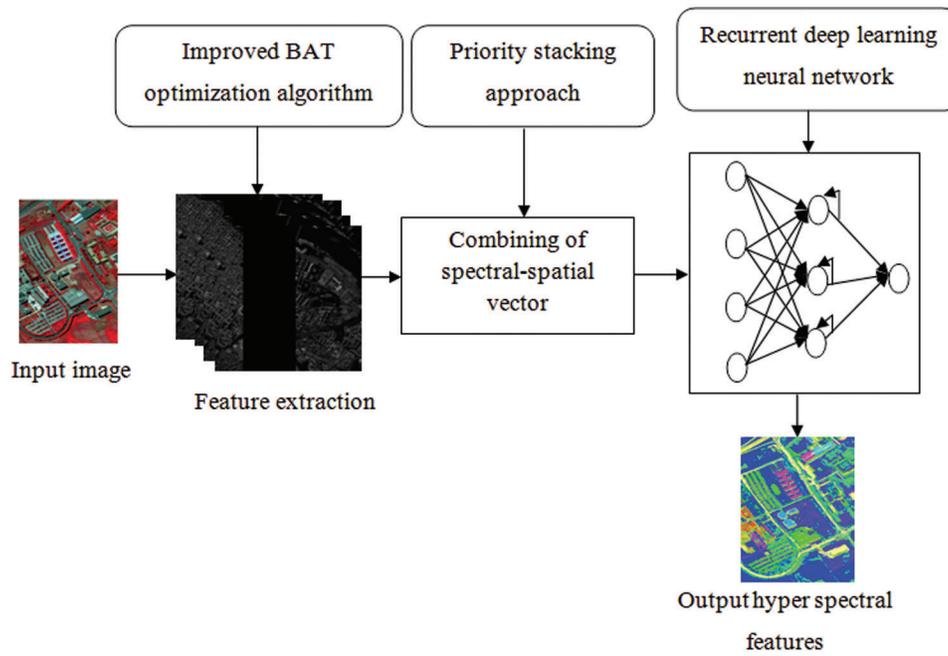

Figure 1: Proposed HDIB scheme

3.3 Feature Extraction Process Using Improved Bat Optimization

Bat Algorithm (BA) is a metaheuristic methodology which is based on the reverberation vacillating activities of bats. Normally the bats analyze and identify their prey using their echolocation attributes. Likewise, the hypersensor is used to sense the HS features which is first analyzed and later senses the object. So here we are using improved bat optimization technique. For the sake of straightforwardness, the subsequent unrealistic guidelines are demarcated:

1. All bats exploit echo oscillation, besides the dissimilarity amongst prey as well as circumstantial barricades are recognized by means of their uniqueness in several enchanted mode;
2. Bats move arbitrarily by way of velocity V_i at position P_i, additionally all bats have a solid frequency f_{min} fluctuating wavelength λ in addition to loudness A_0 to prey. They might perceptively precise the wavelength (otherwise frequency) of their emanated pulses. Moreover, bats remain capable to amend the pulse emission rate $r \in [0, 1]$ based on the type and distance of the prey.
3. Owing to the loudness, here we consider that the loudness variation from a large progressive value A_0 to a minutest perpetual value A_{min}.

For effortlessness, the characteristic plus rate arrays for bats remain customary amongst 0 in addition to 1, where 0 stances for no pulses at all and 1 stand for the pulse emanation.

3.3.1 Movement of Virtual Bats

Here, for extracting the HS images and to get the pure pixels, we initialize the following parameters. To deal with the glitches, the simulated bats remain castoff besides the guidelines that appraise new clarifications

P_i^t besides velocities V_t^i at time phase t rationalized in a multidimensional space which are demarcated by the succeeding formulations.

$$f_t = f\left(fmin_{max}\alpha\right)_{min} \tag{1}$$

$$V_j^i(t) = v_j^i(t-1) + \left|P^i - P_j^j(t-1)\right|f_i \tag{2}$$

$$P_j^i(t) = P_j^i(t-1) + V_j^i(t) \tag{3}$$

3.3.2 Pulse Emission and Loudness

The HS image is sensed by the sensor and it is extracted to get the pure pixels. Likewise, the bat is searching their prey with help of echolocation attributes, in the course of the penetrating progression; *bi* would emanate pulse with huge loudness besides trivial frequency. Formerly BA_i has found its prey, the loudness besides frequency could be modernized as trails:

$$Pu_i^{t+1} = \beta \times A_i^t \tag{4}$$

$$L_i^{t+1} = r_l^0[1 - \exp(-\gamma \times t)] \tag{5}$$

where, BA_i is Bat and pulse emission of bats is Pu_i^{t+1} and loudness at time step t is represented in L_i^{t+1}. There is same value as β and γ.

3.3.3 Feature Selection and Extraction

The customary BA just might be used to resolve various optimization problems like function optimization. Nevertheless, in the case of feature selection, some strategies would be familiarized to elucidate the crusade of bats in the n-dimensional Boolean framework. In the Bat optimization algorithm, we project a binary description of BA for feature selection and the Improved Bat Optimization (IBO) algorithm practices a sigmoid utility to constrain the location of bats to only binary assessment.

$$S_i\left(v_j^i\right) = \frac{1}{1 + \exp\left(-v_j^i\right)} \tag{6}$$

Instead of Eq. (3) the bats position can be updated as following Eq. (7),

$$P_j^i = \begin{cases} 1 & if\ s_i\left(v_j^i\right) > \sigma \\ 0 & otherwise \end{cases} \tag{7}$$

where $\sigma \sim U\ (0, 1)$. Consequently, each bit of bats might be constrained to only binary values, which might designate the occurrence or nonappearance of the structures.

3.3.4 Fitness Function

The BA exploits a fitness function to replicate the convergence of various classes (signified by D_1), of the consistency feature, besides the dispersion of inter classes (symbolized by D_2) of dissimilar features, which is demarcated as (8).

$$Fitness = \frac{\min(D_2(P))}{1 + \max(D_1(Q))} \tag{8}$$

where, $Q = 1, 2, ..., NC$ and $P = 1, 2, ..., C_{NC}^2$ are represented number of texture modules. Nc is the number of interclass. $D_2(Q)$ is the intra-class square inaccuracy of the Qth texture class, $D_2(P)$ is an inter-class square inaccuracy, mentioned in (9) and (10)

$$D_1(Q) = \frac{\sum_{k=1}^{n} (Te_k - u_q)^2}{sn} \qquad (9)$$

$$D_2(P) = W_a \times W_b \times (u_a(p) - u_b(p))^2 \qquad (10)$$

where the number of samples of Qth texture class is represented as sn. Te_k is Texture energy of kth Sample of Qth texture class and u_q its average value sample $u_a(P)$ and $u_b(P)$ is mean value of ath and b^{th} samples of texture class and w_a and w_b is total number of samples of ath and b^{th} texture class.

3.4 Merging Spectral Vector Through Spatial Vector by Means of Priority Stacking Methodology

For improving the quality of images and combining the multiple classification models, we use the priority stacking approach.

3.4.1 Priority Scheduling of Spatial Vector

In this technique, the processes are implemented, with the end objective, that the practice having utmost noteworthy needed to be executed first. Centered on implementation of each technique, the allotment time besides turnaround time is unwavering, for example First Come First Serve (FCFS). For each point p on the limit δ, we fixed a square pixel ϕ_p with the inside p. Specifically, we observe a set of spatial vectors (preparing tests) pixel size with 9×9 pixels.

Calculating the precedence $P(p)$ for each patch,

$$P(p) = C(p)D(p) \qquad (11)$$

where, $C(p)$ and $D(p)$ are confidence term and data term, which given below:

$$C(p) = \frac{\sum_{q \in \phi} \cap \bar{\rho} C(p)}{|\phi_p|} \qquad (12)$$

$$D(p) = \frac{|\nabla_p.n_p|}{\alpha} \qquad (13)$$

where $\bar{\rho}$ is the harmonizing set of objective region ρ, $|\phi_p|$ is patch area, ψ_p, n_p is an unit vector orthogonal to borderline δ and it is a spatial vector besides α is regularization parameter.

If case there is an additional training of the image adjoining the pixel p, $C(p)$ would attain an updated value. In precise, the initialization is that $C(p) = 0$, $\forall p \in \rho$, in addition $D(p) = -1$, $\forall p \in \bar{\rho}$, which ρ is the objective region.

Choosing training samples ϕ_p with the uppermost priority, in addition filling the patch by penetrating the utmost comparable patch after basic image φ. The succeeding equivalence is castoff to denote the resemblance amongst two training illustrations,

$$\phi_q = \arg \min_{\phi q \in \varphi} d\left(\phi_p, \phi_q\right) \qquad (14)$$

Every pixel p′, p′ $\in \phi_p \cap \rho$, is occupied by conforming pixel in ϕ_p besides apprising the assurance value with the subsequent Eq. (15),

$$C(q) = C(p), \forall_q \in \psi_p \cap \rho \qquad (15)$$

3.4.2 Stacking Approach

Stacking is another grouping strategy that is used to link the enormities of a few characterization strategies utilizing a meta-classifier. The proposed methodology is exploited, at the principal level of grouping. Subsequently, the order of potentials with various component congregations, and the consequences of the finest classifier results are stacked using the requisite calculation. In the wake of assembling the potential results, basic classifiers are applied to the blend of these results and the picture includes in the investigations, stacking techniques are independently applied to each level Fig. 2 and Three stacking methodologies (stacking on the main level, stacking on the subsequent level, and stacking on the two levels) and characterization without stacking are looked at. We utilized three stacking techniques to join the characterization yields of the single grouping models.
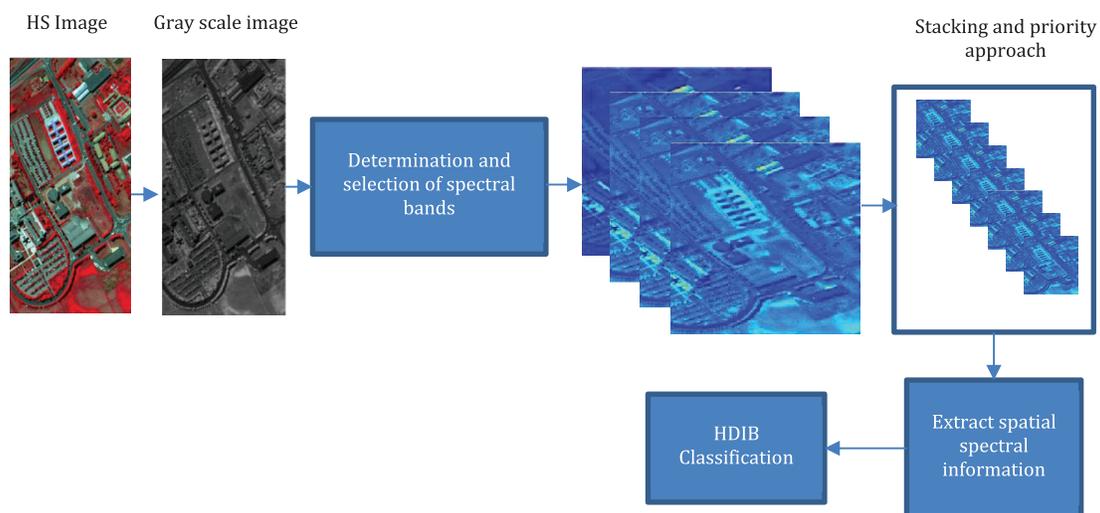

Figure 2: Merging spatial vector with spectral vector by means of priority stacking method

3.5 Classification of HS Images Using Recurrent Deep Learning Neural Network

We propose a novel and a repetitive deep learning neural system architecture for classifying the HS images. The outline of the deep learning neural system is given in Fig. 3. It comprises of two sections: The intermittent portion removes semantic portrayals from pictures; the deep neural part mockups picture/mark affiliation. The likelihood of prediction can be registered by the intermittent deep learning neural system. The picture, mark and intermittent portrayals are anticipated to a similar low dimensional space to demonstrate the picture content relationship. The repetitive deep learning neural system model is utilized; at this point ground-breaking portrayal marks the co-event dependence. It grosses the embedding of the anticipated mark at every time besides keeps up a masked state to display the name on the co-event data. From the probability of the name given, the newly anticipated marks can be figured by their advert frameworks with the aggregate of the image and repetitive embedding. The likelihood of a prediction can be acquired as the result of an earlier likelihood of each mark given the past names in the expectation way.
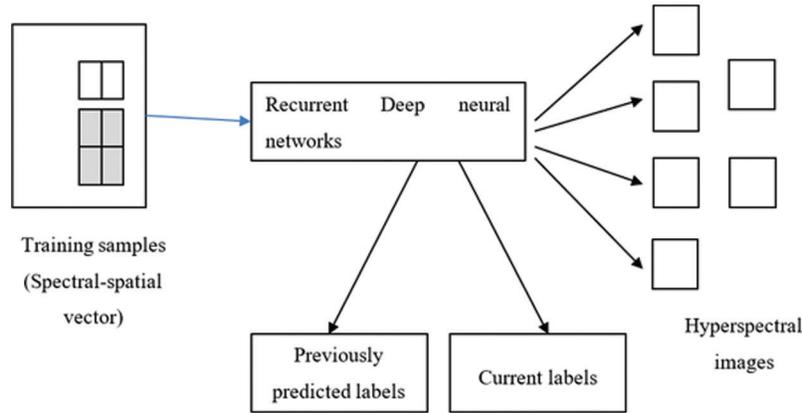
Figure 3: Recurrent deep neural networks classify the hyperspectral images with help of comparing the previous predicted labels and current labels

In a characteristic recurring network as shown in Fig. 3, categorization by means of length S, hidden layer aspect $h^{(s)}$ and the output label $Y^{(s)}$ at the state $s \in [1, \cdots, S]$ might be described as:

$$h^{(s)} = fh\left(W_{hh}h^{(S-1)} + W_{ih}x^{(S)} + bh\right) \tag{16}$$

$$Y^{(s)} = f_0\left(W_{h_0h}h^{(S)} + b_0\right) \tag{17}$$

where, $x^{(s)}$ is the s-th input data, $h^{(s)}$, is the hidden layer unit, $Y^{(s)}$ embodies the output, W_{ih}, W_{hh}, W_{ho} are the revolution matrices amongst $x^{(s)}$ in addition $h^{(s)}$, $h^{(s-1)}$ as well as $h^{(s)}$, besides $Y^{(s)}$. b_h, b_0 are the persistent bias terms, whereas f_h, f_0 are the non-linear stimulation functions.

The label k is signified as a one-hot vector $e_k = [0, \ldots 0, 1, 0, \ldots, 0]$, which is 1 at the k-th position, and 0 at some other location. The label implanting might be attained by burgeoning the one-hot vector with a label entrenching matrix u_l.

$$W_k = u_l.e_k \tag{18}$$

The intermittent layer grosses the label embedding of the prophesied label, by nonlinear utilities:

$$o(t) = h_0(r(t-1), W_k(t),), r(t) = h_r(r(t-1), w(t)) \tag{19}$$

where r (t) besides o (t) are the hidden states in addition to the output of the contemporary layer at the time phase t, correspondingly, wk (t) is the label implanting of the t-th label in the prophecy track, $h_0(.)$ and $h_r(.)$ are the non-linear RNN functions.

$$x_t = h\left(u_0^y o(t) + u_I^y I\right) \tag{20}$$

The matrices for repeated deep layer output besides pixel depiction is $\left(u_0^y, u_I^y\right)$ amount of columns of u_0^y and u_I^y remain the similar as the label embedding matrix u_l. I is the DNN training set, which is from priority stack approach representation. Finally, the label marks might be calculated by proliferating the reverse of u_l beside x_t to total the distances amongst x_t and every label implanting.

$$S(t) = u_I^T x_t \tag{21}$$

The label possibility might be computed by means of Softmax normalization.

4 Performance Analysis

Authors are required to adhere to this Microsoft Word template in preparing their manuscripts for submission. It will speed up the review and typesetting process. Our proposed HDIB design is synthesized and simulated in TensorFlow. Initially, we differentiate the pure pixels of HS images from spectral-spatial features using the improved bat optimization algorithm and further improve the quality of those pixels using spatial vectors as training samples, with help of priority stacking approach. We improve the accuracy and classify the HS images with help of recurrent DNN. We can use TensorFlow for simulating and compressing the HS images, the details of which are shown in Tab. 1. The simulation results are compared with the existing methods like DML, CNN and S+ LP (Single Layer Perceptron) classifiers. The CNN technique encompasses five stages: the full connection layer, the input layer, the max pooling layer, the convolutional layer and the output layer. The simulation and synthesis are done by TensorFlow, the performance of the proposed HDIB algorithm is also shown in Tab. 1.

Table 1: Number of training and testing samples for tamilnadu hills scenes data set

No.	Class	Training	Testing
1	Grass-pasture	200	793
2	Grass-trees	200	1,043
3	Woods	200	1,083
4	Trapezoidal areas	200	433
5	Trees	200	20,445
6	Bare soil	200	4,523
7	Soybean	200	1,230
8	Corn	200	2,578
9	Buildings-grass-trees-drives	200	1,458

4.1 Data Set and Testing Details

4.1.1 Tamilnadu Hills Scenes

The dataset comprises of 145×145 pixels with 224 spectral replication bands with wavelength of 0.4 $-2.5 \times 10^{(-6)}$ m. The investigational groupings accessible for the scrutiny are classified into sixteen groupings. The dataset encompasses 10,249 labeled pixels, out of which 9 classes have been considered. The training and testing statistics are enumerated in Tab. 1. The pseudo-color map and the RS image are illustrated in Fig. 4.

4.1.2 Pavia University Scene

The Pavia University dataset is captured by the Reflective Optical System Imaging Spectrometer (ROSIS-03) optical radar in a municipal region nearby the University of Pavia in Italy & it consists of 115 spectral bands, besides infrared spectra remain enclosed, with wavelength in the range of 430–860 nm. This HS image comprises of 610×340 pixels having a spatial perseverance of 1.3 m. A total of 42,776 labels, as well as 9 groupings are considered. The training and testing statistics are enumerated in Tab. 2. The pseudo-color map and the RS image are shown in Fig. 5.

(a)   (b)   (c)   (d)   (e)
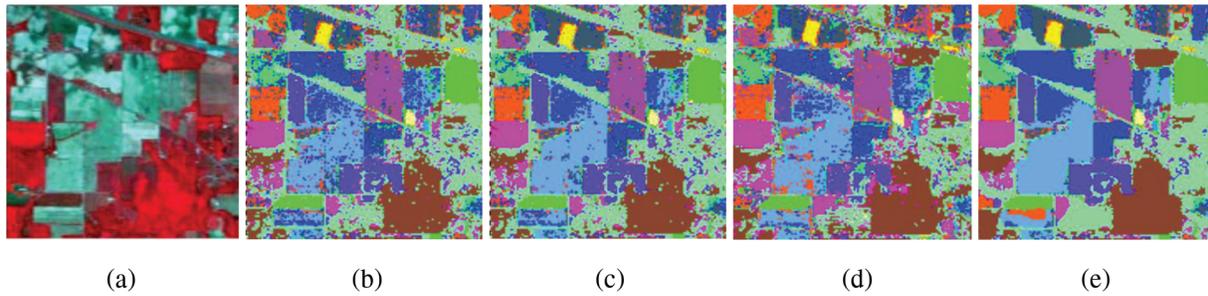
Figure 4: Tamilnadu hills scene (a) input hyper spectral image (b) output of SLP classifier (c) CNN classifier (d) DML classifier (e) proposed HDIB classifier

Table 2: Number of training and testing samples for pavia university scene

No.	Class	Training	Testing
1	Asphalt	200	565
2	Bricks	200	13,900
3	Metal sheets	200	345
4	Bare soil	200	7,421
5	Trees	200	13,445
6	Gravel	200	8,523
7	Meadows	200	14,342
8	Bitumen	200	1,000
9	Shadows	200	548

(a)   (b)   (c)   (d)   (e)
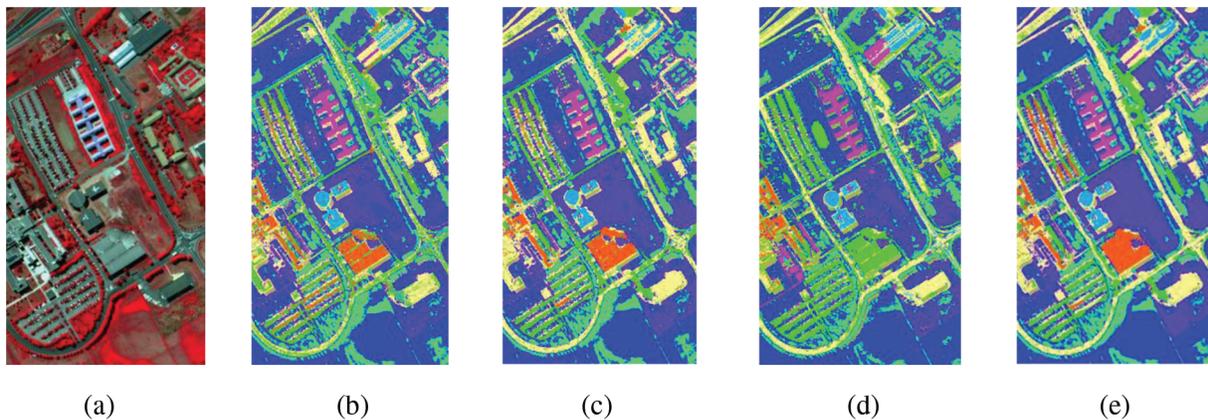
Figure 5: Pavia University scene (a) Three-band color composite image (b) output of SLP classifier (c) CNN classifier (d) DML classifier (e) proposed HDIB classifier

4.1.3 Salinas Scene

The Salinas dataset is captured using the AVIRIS radar, apprehending an extent over Salinas Valley, California, having a spatial resolution of 3.7 m and the dataset consists of 204 bands. It primarily covers

soils, vegetation etc…. and there are 16 diverse land varieties. The training and testing statistics are itemized in Tab. 3. The RS image and the outputs with various techniques are illustrated in Fig. 6

Table 3: Number of training and testing samples for salinas dataset

No.	Class	Training	Testing
1	Brocoli green weeds 1	200	1809
2	Brocoli green weeds 2	200	3521
3	Fallow rough plow	200	1194
4	Corn senesced green weeds	200	3807
5	Lettuce romaine 4wk 200 868	200	868
6	Lettuce romaine 5w	200	1727
7	Vinyard untrained	200	3379
8	Grapes untrained	200	11,701
9	Fallow smooth	200	2478
10	Fallow	200	1976
11	Stubble	200	3959
12	Celery	200	3579
13	Corn_senesced_green_weeds	200	3278
14	Lettuce_romaine_6wk	200	916
15	Lettuce_romaine_7wk	200	1070
16	Vinyard_vertical_trellis	200	1807

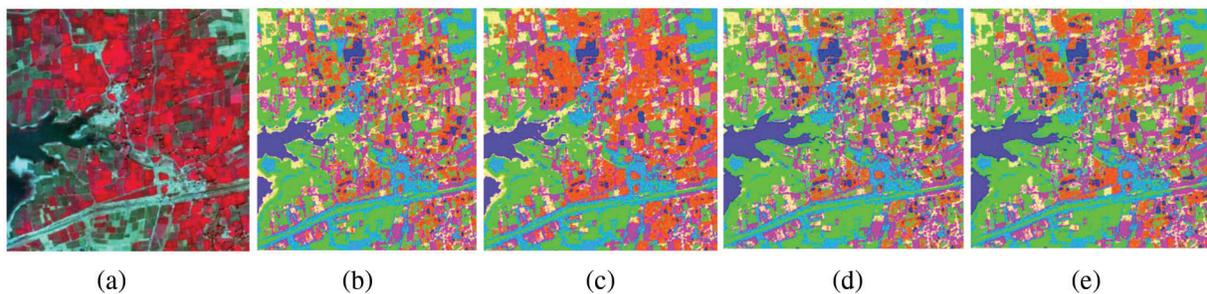(a)　　　　　(b)　　　　　(c)　　　　　(d)　　　　　(e)

Figure 6: Salinas scene (a) Three-band color composite image (b) output of SLP classifier (c) CNN classifier (d) DML classifier (e) proposed HDIB classifier

5 Results and Discussion

The proposed HDIB is compared with existing methods and it uses three data sets. Fig. 4a shows the input HS image of the Tamilnadu hill scene. Figs. 4b–4d shows the classification result of existing classifiers like SLP, CNN and DML. Fig. 4e shows the classification output of proposed HDIB method. Considering the results, one might perceive that SLP did slightly better than the DML besides both approaches have comparable difficulties of misclassification of built-up land and agronomic area. The

usage of spatial information in addition to homogenization of solitary pixels in much enhanced outcomes for the HDIB classifier.

Fig. 5a refers to the HS image from the Pavia University scene data set. Figs. 5b–5d shows the classification result of existing classifiers like SLP, CNN and DML. Fig. 5e shows the classification output of proposed HDIB method. The results validate that the HDIB process is more appropriate for the classification of data sets with elevated dimensions.

From the Tab. 4, the proposed HDIB provides high accuracy images and better reliability of classification. Compared with the existing state-of-art techniques such as CNN, S + LP and DML, the proposed HDIB based soil classifier provides higher accuracy. In this analysis, we have considered 5 different classes (Woods, Trees, Bare soil, Corn, Grass–Pastures) in the case of Tamilnadu dataset. For the Pavia University dataset, we have taken Asphalt, Bricks, Metal Sheets, Bare Soil, Trees as the 5 classes for comparison. Finally, for the Salinas dataset Grapes, Brocoli, Lettuce, Bare Soil, Vinyard was selected for comparing the accuracy with the above-mentioned techniques. We create a comprehensive investigation of two parameters: learning rate μ regularization parameter σ with the 3 HS data sets. When $\mu = 10$, the accuracy is 39.07%, 67.52% and 62.89% for three datasets. The intention is that the a large μ creates the DML network tough to congregate to a stable state. By reducing μ, the classification accuracy shows an upward trend. When $\mu = 0.1$, the highest accuracies are attained for the 3 datasets.

Table 4: Accuracy comparison over Benchmark Scenes

Class	Accuracy comparison											
	Tamilnadu hills scene				Pavia University scene				Salinas scene			
	S + LP	CNN	DML	HDIB	S + LP	CNN	DML	HDIB	S + LP	CNN	DML	HDIB
C1	91.21	87.89	95.54	96.34	91.23	78.89	94.23	97.23	99.23	99.72	99.78	99.913
C2	91.84	98.3	93.43	94.23	92.33	89.33	97.43	98.34	93.84	78.46	90.12	98.34
C3	94.15	99.70	99.76	99.87	92.15	89.70	91.76	93.87	99.61	99.45	99.56	99.89
C4	99.70	95.72	96.43	97.55	92.11	95.56	96.34	97.56	86.98	89.63	90.l4	97.98
C5	92.02	90.54	91.34	92.34	78.02	90.23	93.34	91.45	88.90	90.33	91.45	94.39

6 Conclusion

We have proposed a hybrid deep learning-improved BAT optimization algorithm (HDIB) for soil classification using remote sensing hyperspectral features and we extracted the spectral-spatial features by choosing manually pure pixels from HS image and we combined Spectral-spatial vector by the help of priority stacking approach. We classified the HS images by using of recurrent deep learning neural network also we improved the reliability of classification. Finally, the proposed HDIB classifier results are compared with existing classifiers like S + LP, CNN and DML for three different standard datasets. The comparative analysis shows the effectiveness of proposed HDIB classifier in terms of accuracy. For the Tamil Nadu hills scene dataset, out of the 5 classes chosen, HDIB provided better accuracy in the 4 classes, whereas for the Pavia University dataset and the Salinas scene dataset the accuracy was better in all the 5 classes which was chosen. The accuracy of the proposed HDIB classifier is very high compared to the existing classifiers and the higher percentage clearly indicates that the identification of the various classes is consistent and accurate. Hence, in the future, we will focus on developing multi-class soil features classification methods for HS images and further we can work on speeding up the convergence of the algorithm and parameter fine tuning

References

[1] F. F. Tavin, A. Roman, S. Mathieu, F. Baret, W. Liu *et al.,* "Comparison of metrics for the classification of soils under variable geometrical conditions using hyperspectral data," *IEEE Geoscience and Remote Sensing Letters*, vol. 5, no. 4, pp. 755–759, 2008.

[2] M. Shoshany, O. Almog and V. Alchanatis, "Wavelet decomposition for reducing flux density effects on hyperspectral classification," *IEEE Geoscience and Remote Sensing Letters*, vol. 6, no. 1, pp. 38–41, 2008.

[3] R. Prakash, D. Singh and N. P. Pathak, "A fusion approach to retrieve soil moisture with SAR and optical data," *IEEE Journal of Selected Topics in Applied Earth Observations and Remote Sensing*, vol. 5, no. 1, pp. 196–206, 2012.

[4] S. Ahmad, A. Kalra and H. Stephen, "Estimating soil moisture using remote sensing data: A machine learning approach," *Advances in Water Resources*, vol. 33, no. 1, pp. 69–80, 2010.

[5] N. N. Sanchez, J. M. Fernandez, A. Calera, E. Torres and C. P. Gutierrez, "Combining remote sensing and in situ soil moisture data for the application and validation of a distributed water balance model (HIDROMORE)," *Agricultural Water Management*, vol. 98, no. 1, pp. 69–78, 2010.

[6] V. L. Mulder, S. D. Bruin, M. E. Schaepman and T. R. Mayr, "The use of remote sensing in soil and terrain mapping—A review," *Geoderma*, vol. 162, no. 1–2, pp. 1–19, 2011.

[7] W. H. Wei, F. Y. Hong and T. Tiyip, "The research of soil salinization human impact based on remote sensing classification in oasis irrigation area," *Procedia Environmental Sciences*, vol. 10, no. 4, pp. 2399–2405, 2011.

[8] A. Comber, P. Fisher, C. Brunsdon and A. Khmag, "Spatial analysis of remote sensing image classification accuracy," *Remote Sensing of Environment*, vol. 127, no. 4, pp. 237–246, 2012.

[9] E. Chuvieco, L. Giglio and C. Justice, "Global characterization of fire activity: Toward defining fire regimes from earth observation data," *Global Change Biology*, vol. 14, no. 7, pp. 1488–1502, 2008.

[10] P. Harmon, R. Maus and W. Morrissey, "Expert systems: Tools and applications," in *The Software Engineering section*, 1st ed., New York: John Wiley & Sons, Inc, 1988.

[11] D. Rocchini, G. M. Foody, H. Nagendra, C. Ricotta, M. Anand *et al.,* "Uncertainty in ecosystem mapping by remote sensing," *Computers & Geosciences*, vol. 50, no. 359, pp. 128–135, 2013.

[12] C. Hladik and M. Alber, "Classification of salt marsh vegetation using edaphic and remote sensing-derived variables," *Estuarine Coastal and Shelf Science*, vol. 141, pp. 47–57, 2014.

[13] H. K. Winning and M. J. Hann, "Modelling soil erosion risk for pipelines using remote sensed data," *Biosystems Engineering*, vol. 127, pp. 135–143, 2014.

[14] J. Du, J. S. Kimball, M. Azarderakhsh, R. S. Dunbar, M. Moghaddam *et al.,* "Classification of Alaska spring thaw characteristics using satellite L-band radar remote sensing," *IEEE Transactions on Geoscience and Remote Sensing*, vol. 53, no. 1, pp. 542–556, 2015.

[15] O. Rozenstein, T. P. Kagan, C. Salbach and A. Karnieli, "Comparing the effect of preprocessing transformations on methods of land-use classification derived from spectral soil measurements," *IEEE Journal of Selected Topics in Applied Earth Observations and Remote Sensing*, vol. 8, no. 6, pp. 2393–2404, 2015.

[16] Y. Tang and X. Li, "Set-based similarity learning in subspace for agricultural remote sensing classification," *Neurocomputing*, vol. 173, no. 10–12, pp. 332–338, 2014.

[17] M. A. E. A. Rahman, A. Natarajan, C. A. Srinivasamurthy and R. Hegde, "Estimating soil fertility status in physically degraded land using GIS and remote sensing techniques in Chamarajanagar district, Karnataka, India," *The Egyptian Journal of Remote Sensing and Space Science*, vol. 19, no. 1, pp. 95–108, 2016.

[18] L. Zhu and L. Ma, "Class centroid alignment-based domain adaptation for classification of remote sensing images," *Pattern Recognition Letters*, vol. 83, no. 1, pp. 124–132, 2016.

[19] A. B. Neto, C. D. S. B. Bonini, B. S. Bisi and A. R. Reis, "Artificial neural network for classification and analysis of degraded soils," *IEEE Latin America Transactions*, vol. 15, no. 3, pp. 503–509, 2017.

[20] W. Wu, Q. Yang, J. Lv, A. Li and H. Liu, "Investigation of remote sensing imageries for identifying soil texture classes using classification methods," *IEEE Transactions on Geoscience and Remote Sensing*, vol. 57, no. 3, pp. 1–11, 2018.

[21] B. Gao, A. Lu, Y. Pan, L. Huo, Y. Gao *et al.,* "Additional sampling layout optimization method for environmental quality grade classifications of farmland soil," *IEEE Journal of Selected Topics in Applied Earth Observations and Remote Sensing*, vol. 10, no. 12, pp. 5350–5358, 2017.

[22] S. Ghosh, D. Biswas, S. Biswas, D. C. Sarkar and P. P. Sarkar, "Soil classification from large imagery databases using a neuro-fuzzy classifier," *Canadian Journal of Electrical and Computer Engineering*, vol. 39, no. 4, pp. 333–343, 2016.

[23] M. D. Yang, K. S. Huang, Y. F. Yang, L. Y. Lu, Y. Z. Feng *et al.,* "Hyperspectral image classification using fast and adaptive bidimensional empirical mode decomposition with minimum noise fraction," *IEEE Geoscience and Remote Sensing Letters*, vol. 13, no. 12, pp. 1–5, 2016.

[24] B. Xue, C. Yu, Y. Wang, M. Song, S. Li *et al.,* "A subpixel target detection approach to hyperspectral image classification," *IEEE Transactions on Geoscience and Remote Sensing*, vol. 55, no. 9, pp. 5093–5114, 2017.

[25] R. Pike, G. Lu, D. Wang, Z. G. Chen and B. Fei, "A minimum spanning forest-based method for noninvasive cancer detection with hyperspectral imaging," *IEEE Transactions on Biomedical Engineering*, vol. 63, no. 3, pp. 1–11, 2015.

[26] J. Guo, X. Zhou, J. Li, A. Plaza and S. Prasad, "Superpixel-based active learning and online feature importance learning for hyperspectral image analysis," *IEEE Journal of Selected Topics in Applied Earth Observations and Remote Sensing*, vol. 1, no. 1, pp. 347–359, 2017.

[27] W. Li, Z. Wang, Y. Wang, J. Wu, J. Wang *et al.,* "Classification of high spatial resolution remote sensing scenes method using transfer learning and deep convolutional neural network," *IEEE Journal of Selected Topics in Applied Earth Observations and Remote Sensing*, vol. 20, no. 10, pp. 1986–1995, 2020.

[28] X. Tan, Z. Xiao, Q. Wan and W. Shao, "Scale sensitive neural network for road segmentation in high-resolution remote sensing images," *IEEE Geoscience and Remote Sensing Letters*, vol. 18, no. 3, pp. 533–537, 2020.

[29] X. Cao, Y. Ge, R. Li, J. Zhao and L. Jiao, "Hyperspectral imagery classification with deep metric learning," *Neurocomputing*, vol. 356, no. 4, pp. 217–227, 2019.

[30] Q. Liu, Z. Li, S. Shuai and Q. Sun, "Spectral group attention networks for hyperspectral image classification with spectral separability analysis," *Infrared Physics & Technology*, vol. 108, no. 1, pp. 1–24, 2020.

[31] Y. Chu, H. Lin, L. Yang, D. Zhang, Y. Diao *et al.,* "Hyperspectral image classification based on discriminative locality preserving broad learning system," *Knowledge-Based Systems*, vol. 206, no. 6, pp. 1–12, 2020.

[32] X. Meng, Y. Bao, J. Liu, H. Liu, X. Zhang *et al.,* "Regional soil organic carbon prediction model based on a discrete wavelet analysis of hyperspectral satellite data,"*International Journal of Applied Earth Observation and Geoinformation*, vol. 89, no. 1, pp. 1–18, 2020.

[33] S. G. Azar, S. Meshgini, T. Y. Rezaii and S. Beheshti, "Hyperspectral image classification based on sparse modeling of spectral blocks," *Neurocomputing*, vol. 407, no. 12, pp. 12–23, 2020.

[34] O. Okwuashi and C. E. Ndehedehe, "Deep support vector machine for hyperspectral image classification," *Pattern Recognition*, vol. 103, no. 4, pp. 1–28, 2020.

[35] Y. Zhang, Y. Ma, X. Dai, H. Li, X. Mei *et al.,* "Locality-constrained sparse representation for hyperspectral image classification," *Information Sciences*, vol. 546, no. 6, pp. 858–870, 2020.

[36] Z. Zheng and Z. Zhong, "Remote sensing image retrieval with Gabor-CA-ResNet and split based deep feature transform network," *Remote Sensing*, vol. 13, pp. 1–18, 2021.

[37] X. Zhao, H. Li, P. Wang and L. Jing, "An image registration method using deep residual network features for multisource high resolution remote sensing images," *Remote Sensing*, vol. 13, no. 17, pp. 1–22, 2021.

[38] L. Chen, H. Wang and X. Meng, "Remote sensing image dataset expansion based on generative adversarial networks with modified shuffle attention," *Sensors*, vol. 21, no. 14, pp. 1–18, 2021.

[39] F. Zhang, C. Wang, K. Pan and Z. Guo, "The simultaneous prediction of soil properties and vegetation coverage from Vis-NIR hyperspectral data with a one-dimensional convolutional neural network: A laboratory simulation study," *Remote Sensing*, vol. 14, no. 2, pp. 1–15, 2022.